Determination of electrostatic parameters of a coumarin derivative compound $C_{17}H_{13}NO_3$ by x-ray and density functional theory

Youcef Megrouss, Nadia Benhalima, Rawia Bahoussi, Nouredine Boukabcha, Abdelkader Chouaih, and Fodil Hamzaoui†

Laboratoire de Technologie et Propriétédu Solide (LTPS), University of Mostaganem, Mostaganem 27000, *Algeria*

(Received 13 March 2015; revised manuscript received 11 May 2015; published online 20 August 2015)

This work is devoted to the experimental determination of the electrostatic properties of the molecular 4-methyl-7-(salicylidene amino) coumarin ($C_{17}H_{13}NC_3$) using high resolution x-ray diffraction data. The experimental results are compared with those obtained theoretically from calculation type *ab initio*. The experimental investigation is carried out using the molecular electron charge density distribution based on the multipolar model of Hansen and Coppens. However the theoretical calculations are conducted by using the molecular orbital B3LYP method and the Hartree–Fock (HF) approximation with the basis set 6-31G (d,p) implemented in the Gaussian program. In addition to the structural analysis, the thermal agitation is also analyzed in terms of rigid blocks to ensure a better precision of the results. Subsequently, the electrostatic atomic and molecular properties such as the net charges, the molecular dipolar moment to highlight the nature of charge transfer existing within the molecule studied are derived. Moreover, the obtained electrostatic potential enables the localization of the electropositive and the electronegative parts of the investigated molecule. The present work reports in detail the obtained electrostatic properties of this biologically important molecule.

Keywords: electron charge density, electrostatic potential, molecular dipole moment and x-ray diffraction

PACS: 61.50.–f, 61.05.cp, 31.15.A–, 31.15.ap **DOI:** 10.1088/1674-1056/24/10/106103

1. Introduction

The coumarin derivatives have been largely investigated by many researchers for their various biological properties.[1] It has been shown that the biological activity is directly related to the configuration and the charge density distribution around the asymmetric sites of the concerned molecules.[2–4]

In this context, the present work focuses on the study of the molecular electrostatic potential and provides some other electrostatics properties such as the net atomic charges and the molecular dipole moment. Both experimental and theoretical investigations are presented here.

The experimental investigation is based on the x-ray experiment crystal data published previously by Aazam *et al.*[5] In a first stage, in order to improve the accuracy of the crystallographic parameters, structural analysis and thermal motion analysis are performed using the multipolar charge density model of Hansen and Coppens[6] and the rigid-body bond test method respectively.[7] In the second stage, the obtained crystallographic multipolar parameters are used to describe the electron density distribution in the crystal.[8] The electrostatic potential around the molecule is also calculated so as to describe the nature of inter- and intra-molecular charge transfers in this compound.

The theoretical investigation consists of an *ab initio* molecular orbital calculation with using the Becke–Lee–Yang–Part's three-parameter hybrid functional (B3LYP) method and Hartree–Fock (HF) approximation with the basis set 6-31G(d,p) implemented in the Gaussian 03 package.[9] The theoretical and experimental results are compared with each other and found to be in very good agreement.

2. Crystallographic investigation

2.1. Crystal structure refinement

The crystallographic investigation described in the work of Aazam *et al.* is based on spherical atom refinement.[5] In order to improve the accuracy of the results and to determine the molecular charge density distribution, the Hansen-Coppens multipole formalism implemented in the Mopro least squares program for multipole refinement investigations[10] is used. The multipolar model used describes the crystal electron density as a superposition of non-spherical pseudo-atoms modeled using a multipole expansion as:

$$\rho_{\text{atom}}(\boldsymbol{r}) = \rho_{\text{c}}(\boldsymbol{r}) + P_{\text{v}}k'^3\rho_{\text{v}}(k'\boldsymbol{r}) + \sum_{l=0}^{l\max}\sum_{m=-1}^{+1} k''R_1(k''\boldsymbol{r})P_{lm}Y_{lm}\left(\frac{\boldsymbol{r}}{r}\right), \quad (1)$$

where ρ_{c} and ρ_{v} are spherically averaged Hartree–Fock core and valence density respectively, with ρ_{v} being normalized to one electron; $Y_{lm_+^-}$ are the spherical harmonic angular functions that are modulated by the Slater-type radial functions; N_l is a normalization factor. The values for parameters $n = n_l$ and ξ are chosen according to the rules suggested by Coppens (1997).[3] In practice, the expansion and contraction of the valence shell depend on two charge density variables, i.e., the

†Corresponding author. E-mail: fodil_hamzaoui@yahoo.fr

© 2015 Chinese Physical Society and IOP Publishing Ltd

population parameter and a kappa parameter; they are added to the conventional parameters of structure analysis.[5] The population parameters P_v and P_{lm} are floated along with k' and k'' during the refinement, the summation over m in Eq. (1) includes $\pm l$, so that for each one, $2l+1$ functions are included. The aspheric charge density is described at the octupole level ($l=3$) for the atoms C, N, and O and at the dipole levels ($l=1$ or 2) for hydrogen atoms not involved and involved in strong H bonds, respectively. Charge densities of all hydrogen are considered to have cylindrical symmetry along the corresponding hydrogen–heavy atom bond.

The least-square method is used to refine the crystal structure against F^2 using atomic anisotropic thermal parameters for all non-hydrogen atoms. The H atoms are located from a difference Fourier map and included in the refinement with the isotropic temperature factor of the carrier atom. After the thermal motion analysis in terms of the rigid body bond test, the anisotropic temperature factors for the hydrogen atoms are introduced. The accuracies of results are significantly improved: the final refinement R factor decreases to 0.4%. The crystallographic details are given in Table 1.

Table 1. Crystal data and structure refinement details.

Compound empirical formula	4-methyl-7-(salicylideneamino) coumarin $C_{17}H_{13}NO_3$	
Temperature/K	173(2)	
Crystal system, space group	monoclinic, $P21/c$	
Unit cell dimension		
a/Å	8.7209(3)	
b/Å	9.9919(3)	
c/Å	15.3906 (4)	
β/(°)	97.853(2)	
Wavelength/Å	0.71073	
Z, calculated density/g·cm^{-3}	4, 1.396	
Reflections collected/unique	2600/2213	
Least-square multipole refinement factors: N is the number of refined parameters. The atomic scattering factors come from the international tables for x-ray crystallography.		
	N	$R=\Sigma\|Fo\|-\|Fc\|/\Sigma\|Fo\|$ $wR=[\Sigma(\|Fo\|-\|Fc\|)^2/\Sigma w\|Fo\|^2]^{1/2}$
Spherical model[5]	195	3.7% 9.9%
Multipolar model	276	0.4% 1.9%

The general feature of the structure consists of a methyl substituted coumarin group connected to a 2-hydroxyphenyl ring via an azomethine linkage as shown in Fig. 1. The coumarin and benzene ring planes form a dihedral angle of 24.0° indicating an absence of the coupling as reported in the earlier work of Aazam *et al.*[5]

The exploration of the molecular environment within the unit cell gives rise to two types of interactions: the first one concerns a strong $O_1 \ldots H_1 \ldots N_1$ intramolecular hydrogen bond and the second one involves a weak intermolecular hydrogen bond responsible for the crystal package determined by the sites $C_7 \ldots C_7 \ldots C_3$. Table 1 gives the description of the hydrogen bonds spotted in the crystal structure.

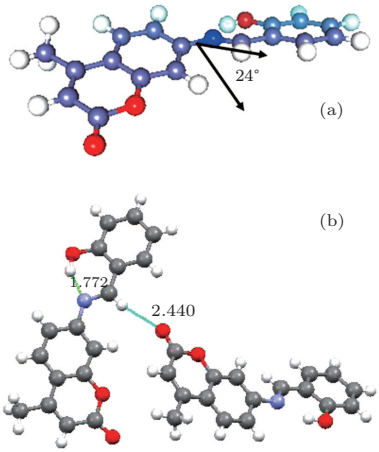


Fig. 1. (color online) Chemical structures of the title compound: (a) the dihedral angle within the molecule. (b) View of the hydrogen bonding.

Table 2. Hydrogen bonds and their properties in 4-methyl-7-(salicylideneamino)coumarin crystal.

D–H···A	D–H/Å	D–A/Å	H–A/Å	D–H···A/Å	Properties
O_1–H_1 N_1 (i)	0.934	2.603	1.763	148.00	strong
C_4–H_4 O_1 (ii)	0.958	3.380	2.643	134.06	weak
C_4–H_4 C_2 (iii)	0.958	3.337	2.633	130.62	weak
C_7–H_7C_3 (iv)	0.954	3.273	2.438	145.96	weak
C_{13}–H_{13} C_3 (iv)	0.954	3.556	2.624	165.44	weak

Equivalent positions:
(i) x, y, z,
(ii) $-x+2$, $+y-1/2$, $-z+1/2+1$,
(iii) x, $-y-1/2$, $+z+1/2$,
(iv) $-x+1$, $+y-1/2$, $-z+1/2$.

2.2. Thermal motion analysis

The thermal motion analysis of 4-methyl-7-(salicylideneamino) coumarin is performed using the THMA11 program.[7] The rigid-body motion is described by three tensors, $\boldsymbol{T}$ for the translation, $\boldsymbol{L}$ for the liberation, and $\boldsymbol{S}$ when taking into account the correlation between translation and liberation. These tensors are obtained by a least-square fit refinement by using the observed atomic thermal motion parameters obtained from the x-ray refinement reported in Table 4. In the rigid body bond model, the bonded pairs of the non-H atoms are assumed to have differences between the mean-square displacement amplitudes (MSDAs) along the interatomic directions $\Delta \leq 10.10^{-4}$ Å^2.[8] For all pairs of atoms in the molecule, the MSDAs Δ_{AB} in the AB direction are calculated and reported in Table 3.

Table 3. Atomic displacement parameters in units of Å^2.

	U_{11}	U_{22}	U_{33}	U_{12}	U_{13}	U23	
O_1	0.0323	0.0331	0.0320	–0.0070	–0.0099	0.0040	OBSERVED
	0.0357	0.0357	0.0297	–0.0067	–0.0091	0.0076	CALCULATED
C_2	0.0376	0.0256	0.0232	–0.0011	–0.0089	0.0015	OBSERVED
	0.0361	0.0290	0.0254	–0.0015	–0.0070	0.0014	CALCULATED
C_3	0.0589	0.0383	0.0301	–0.0048	–0.0182	0.0055	OBSERVED
	0.0588	0.0375	0.0308	–0.0045	–0.0157	0.0067	CALCULATED
N_1	0.0324	0.0261	0.0234	–0.0023	–0.0024	0.0025	OBSERVED
	0.0262	0.0257	0.0222	–0.0021	–0.0023	–0.0007	CALCULATED
C_1	0.0242	0.0246	0.0218	0.0007	0.0020	–0.0009	OBSERVED
	0.0258	0.0247	0.0241	0.0004	0.0009	–0.0006	CALCULATED
C_2	0.0231	0.0273	0.0252	–0.0003	0.0021	–0.0006	OBSERVED
	0.0282	0.0293	0.0253	–0.0004	–0.0006	0.0030	CALCULATED
C_3	0.0290	0.0333	0.0283	0.0042	–0.0015	0.0050	OBSERVED
	0.0292	0.0315	0.0281	0.0016	0.0019	0.0055	CALCULATED
C_4	0.0361	0.0260	0.0356	0.0042	0.0064	0.0071	OBSERVED
	0.0285	0.0270	0.0288	0.0042	0.0071	0.0027	CALCULATED
C_5	0.0313	0.0258	0.0367	–0.0029	0.0054	–0.0015	OBSERVED
	0.0320	0.0246	0.0321	0.0004	0.0031	0.0010	CALCULATED
C_6	0.0265	0.0297	0.0262	–0.0010	–0.0005	–0.0031	OBSERVED
	0.0303	0.0245	0.0302	–0.0014	–0.0005	0.0003	CALCULATED
C_7	0.0274	0.0276	0.0205	0.0003	–0.0023	0.0004	OBSERVED
	0.0249	0.0242	0.0231	–0.0007	–0.0010	–0.0014	CALCULATED
C_8	0.0273	0.0265	0.0238	–0.0014	–0.0009	0.0029	OBSERVED
	0.0256	0.0250	0.0220	–0.0021	–0.0022	–0.0012	CALCULATED
C_9	0.0412	0.0337	0.0231	–0.0089	–0.0069	0.0010	OBSERVED
	0.0369	0.0270	0.0243	–0.0068	–0.0055	–0.0003	CALCULATED
C_{10}	0.0373	0.0275	0.0265	–0.0083	–0.0031	–0.0018	OBSERVED
	0.0375	0.0264	0.0257	–0.0064	–0.0037	–0.0003	CALCULATED
C_{11}	0.0244	0.0246	0.0242	–0.0007	0.0021	–0.0003	OBSERVED
	0.0262	0.0252	0.0244	–0.0009	0.0001	–0.0003	CALCULATED
C_{12}	0.0242	0.0266	0.0199	0.0012	–0.0016	–0.0006	OBSERVED
	0.0254	0.0255	0.0232	0.0000	–0.0019	–0.0004	CALCULATED
C_{13}	0.0281	0.0228	0.0249	–0.0013	–0.0018	–0.0012	OBSERVED
	0.0255	0.0248	0.0224	–0.0007	–0.0025	–0.0013	CALCULATED
C_{14}	0.0243	0.0280	0.0015	0.0042	0.0015	0.0243	OBSERVED
	0.0259	0.0268	0.0008	0.0026	0.0011	0.0259	CALCULATED
C_{15}	0.0265	0.0296	0.0008	–0.0003	0.0054	0.0265	OBSERVED
	0.0284	0.0272	0.0032	0.0013	0.0029	0.0284	CALCULATED
C_{16}	0.0294	0.0265	0.0018	–0.0040	0.0048	0.0294	OBSERVED
	0.0313	0.0272	–0.0001	–0.0065	0.0036	0.0313	CALCULATED
C_{17}	0.0253	0.0314	–0.0032	0.0025	0.0014	0.0253	OBSERVED
	0.0262	0.0314	–0.0034	0.0028	0.0016	0.0262	CALCULATED

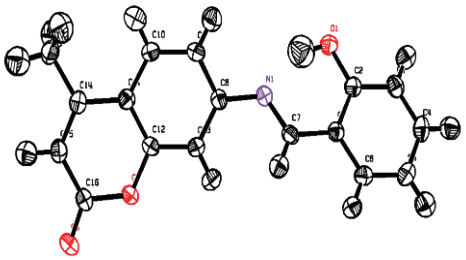


Fig. 2. (color online) MoPro diagram: thermal ellipsoids are shown for the 50% probability level.

In the general treatment of the molecular thermal motion in terms of rigid-body ($\boldsymbol{TLS}$) the calculated anisotropic thermal parameters are given in the Trueblood notation such as:[11]

$$U_{IJ} = T_{IJ} + G_{IJKL}L_{KL} + H_{IJKL}SKL + D^2\Omega^2_{ninj}, \qquad (2)$$

where G, and D are geometrical parameters. The last term on the right-hand side of Eq. (2) is related to any additional intralibration (Ω) around a chosen axis. The rigid-body fit suggests one independent liberation axis around the bond C(8)–N(1). The thermal motion of the H atoms takes into account two contributions. The first one is due to the rigid molecular motion and the second one comes from the C–H vibrations.[12,13] The T, L, and S tensors obtained from the least-square fitting are given in Table 5. The C–H bond frequencies of the molecule are cited from Baert *et al.*'s work.[14] The results of the thermal motion parameters of the H atoms are summarized in Table 6. Using the MoPro viewer diagram,[15] the ellipsoids of the different atoms representing their thermal motion described above are shown in Fig. 2.

Table 4. Matrix for differences in MSDA (mean square displacements of atoms): values listed are 10^4 MSDAs for column atom minus that for row atom.

	C_{17}	C_{16}	C_{15}	C_{14}	C_{13}	C_{12}	C_{11}	C_{10}	C_9	C_8	C_7	C_6	C_5	C_4	C_3	C_2
O_1																9
C_2		4				4										
C_3										1	11					
C_5												4				
C_1											1	15				14
C_2															–7	
C_3														12		
C_4													–13			
C_5												4				
C_8					3											
C_9																
C_{10}							–2									
C_{11}						11	–6									
C_{12}					–7											
C_{13}																
N_1										1	9					
C_{14}	0		–2													

Table 5. Rigid body vibration parameters of the $\boldsymbol{T}$, $\boldsymbol{L}$, and $\boldsymbol{S}$ tensors.

$\boldsymbol{T}$	$\boldsymbol{L}$/Å^2	$\boldsymbol{S}$/rad·Å
$\begin{pmatrix} 0.02425 & -0.00103 & -0.00185 \\ & 0.02446 & -0.00149 \\ & & 0.02188 \end{pmatrix}$	$\begin{pmatrix} 0.00005 & 0.00007 & -0.00035 \\ & 0.00324 & -0.00217 \\ & & 0.00157 \end{pmatrix}$	$\begin{pmatrix} 0.00035 & -0.00007 & 0.00013 \\ 0.00007 & -0.00051 & 0.00050 \\ 0.00009 & 0.00037 & 0.00015 \end{pmatrix}$

Table 6. Thermal vibration parameters for the H atoms calculated from the $\boldsymbol{TLS}$ group tensors plus the internal C–H bond vibration.

Atom	U_{11}	U_{22}	U_{33}	U_{12}	U_{13}	U_{23}
H_1	0.0316	0.0328	0.0274	–0.0057	–0.0044	0.0050
H_3	0.0332	0.0384	0.0331	0.0006	0.0019	0.0114
H_4	0.0325	0.0283	0.0315	0.0066	0.0142	0.0046
H_5	0.0391	0.0256	0.0395	–0.0026	0.0056	0.0027
H_6	0.0339	0.0267	0.0366	–0.0057	–0.0017	0.0025
H_7	0.0256	0.0249	0.0268	–0.0023	0.0000	–0.0003
H_9	0.0472	0.0302	0.0265	–0.0119	–0.0073	0.0012
H_{10}	0.0496	0.0282	0.0290	–0.0114	–0.0032	0.0005
H_{13}	0.0304	0.0256	0.0235	–0.0022	–0.0020	–0.0012
H_{15}	0.0288	0.0298	0.0292	0.0053	0.0070	0.0047
$H_{17}A$	0.0382	0.0301	0.0379	–0.0074	0.0015	0.0057
$H_{17}B$	0.0563	0.0253	0.0311	–0.0050	0.0092	–0.0002
$H_{17}C$	0.0397	0.0263	0.0330	0.0000	0.0115	0.0026

3. Theoretical *ab initio* investigation

In order to investigate the theoretical calculations of the molecular structure parameter the *ab initio* methods are adopted. These calculations are performed with the density functional theory (DFT) at B3LYP (Becke's three-parameter hybrid functional using the correlation functional of Lee, Yang, and Parr, which includes both local and non-local terms in the correlation functional) method at the 6-31G* level using the Gaussian 03 computational chemistry program package.[9] The parameters of the optimized structure (bond lengths and bond angles) are listed in Tables 7 and 8 respectively. It has

been observed that all the calculated parameters are in accordance with the x-ray results. In spite of the differences, the determined geometric parameters represent a good approximation which enables the calculation of other parameters, such as the vibrational wave numbers. It should be noted that some of the optimized bond lengths and bond angles have slightly different values from the corresponding experimental ones due to the fact that the theoretical calculations consider only isolated molecules in the gaseous phase while the experimental results refer to molecules in a crystal environment.

Table 7. Bond lengths of 4-methyl-7-(salicylideneamino) coumarin in units of Å.

Atom 1	Atom 2	Distance		
		x-ray	DFT	HF
O_1	C_2	1.349	1.361	1.354
C_3	C_{16}	1.212	1.229	1.207
C_2	C_3	1.394	1.403	1.390
C_4	C_5	1.395	1.409	1.395
C_9	C_{10}	1.376	1.386	1.376
C_{14}	C_{15}	1.348	1.364	1.342
N_1	C_7	1.288	1.307	1.275
C_1	C_2	1.413	1.427	1.401
C_{11}	C_{14}	1.450	1.456	1.463
C_{14}	C_{17}	1.495	1.507	1.503
C_1	C_6	1.403	1.414	1.400
C_3	C_4	1.379	1.391	1.379
C_5	C_6	1.379	1.388	1.377
C_8	C_9	1.399	1.413	1.399
C_{10}	C_{11}	1.399	1.413	1.400
C_{12}	C_{13}	1.384	1.393	1.382
C_2	C_{16}	1.380	1.428	1.378
C_1	C_7	1.448	1.442	1.455
C_8	C_{13}	1.390	1.402	1.386
C_{15}	C_{16}	1.441	1.449	1.453

Table 8. Bond angles of 4-methyl-7-(salicylideneamino) coumarin in units of (°).

Atom 1	Atom 2	Atom 3	Distance		
			x-ray	DFT	HF
C_{16}	C_2	C_{12}	121.50	122.10	123.80
C_8	N_1	C_7	120.89	123.04	123.12
C_2	C_3	C_4	120.33	119.95	120.04
C_5	C_4	C_3	120.92	120.99	120.78
C_1	C_6	C_5	121.38	121.05	121.40
C_1	C_7	N_1	121.43	121.84	123.35
C_{10}	C_9	C_8	120.57	120.47	120.35
C_{11}	C_{10}	C_9	121.29	121.18	121.05
C_8	C_{13}	C_{12}	118.77	119.36	119.03
C_{16}	C_{15}	C_{14}	123.06	123.59	122.76
C_2	C_1	C_6	118.72	118.78	118.59
C_2	C_1	C_7	121.50	120.84	122.35
C_6	C_1	C_7	119.78	120.36	119.04
O_1	C_2	C_1	118.76	121.24	122.44
O_1	C_2	C_3	119.55	118.91	117.43
C_4	C_5	C_6	119.11	119.36	119.04
N_1	C_8	C_{13}	123.68	123.21	122.88
C_9	C_8	C_{13}	119.52	119.39	119.59
C_8	C_9	C_{10}	120.57	120.47	120.35
C_2	C_{16}	C_3	116.40	117.44	118.64
C_1	C_2	C_3	119.55	119.59	120.11
C_4	C_5	C_6	119.11	119.08	119.04
N_1	C_8	C_9	116.76	116.76	117.49
C_{10}	C_{11}	C_{12}	116.87	116.88	117.32
C_{10}	C_{11}	C_{14}	124.43	124.40	124.60
C_{12}	C_{11}	C_{14}	118.70	118.70	118.06
C_2	C_{12}	C_{11}	121.23	121.27	120.52
C_2	C_{12}	C_{13}	115.79	115.73	116.85
C_{11}	C_{12}	C_{13}	122.98	122.98	122.62
C_{11}	C_{14}	C_{15}	118.32	118.31	119.27
C_{11}	C_{14}	C_{17}	120.46	120.45	119.62
C_{15}	C_{14}	C_{17}	121.22	120.85	121.09
C_{14}	C_{15}	C_{16}	123.07	123.10	122.76
C_2	C_{16}	C_{15}	117.19	117.16	115.57
C_3	C_{16}	C_{15}	126.41	126.45	125.77

4. Results and discussion

4.1. Electron density maps

The non-spherical atom model used in multipole refinement gives structure factor phases closer to the true phases for crystals than the spherical model does. This enables the mapping of the electron density distribution by using difference Fourier synthesis to observe the experimental charge density deformation of the molecule.

Figure 3 shows the electron charge density distributions in two different planes of the molecule: the first plane (a) formed by the electro-acceptor group (2-hydroxyphenyl), and the second plane (b) containing the electro-donor group (coumarin). In these figures, one can observe the absence of the density on the atomic sites and the appearance of all the bond density peaks as expected in the literature. These maps show a first confirmation concerning the high quality of the data sets and the efficiency of the used model of Hansen and Coppens.[6]

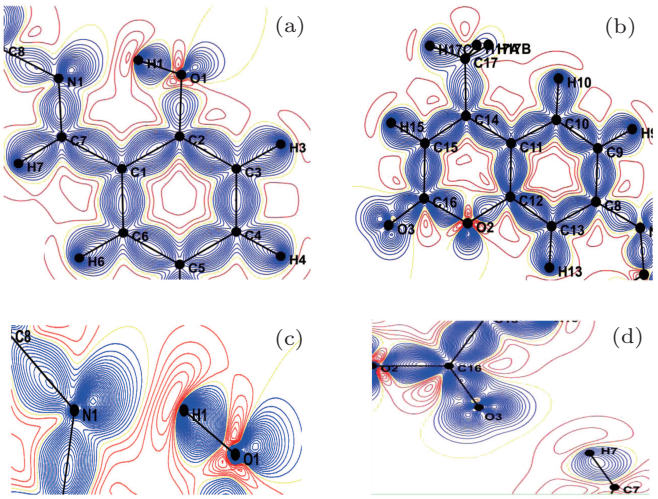


Fig. 3. (color online) Deformation density maps with a contour interval of 0.05 eÅ^{-3}, positive density in blue, and negative density in red: (a) plane of the 2phenol amino, (b) the coumarin plane, (c) in the plane of intramolecular hydrogen bond $N_1 \ldots H_1 \ldots O_1$, and (d) in the plane of the intermolecular hydrogen bond $C_7 \ldots H_7 \ldots O_3$.

4.2. Electrostatic molecular properties

The knowledge of the analytical function of the electron density distribution produced by high resolution x-ray experiment, could give rise to some important molecular electrostatic properties such as the atomic net charges, the molecular dipole moment, and the electrostatic potential around the molecule.

4.3. Net atomic charges

The partial charges on the different atoms are estimated by using the valence population coefficients p_v^i according to the following equation $q_i = n_i - p_v^i$ where n_i is the total number of electrons of atom i. The population coefficients are presented in Table 9. The refined atomic charges have the signs generally determined by the chemical knowledge: H atoms are positively charged, whereas O and N atoms are negatively charged. In Table 8 the theoretical net charges are also reported. It can be observed that experimental and theoretical results are in agreement.

Table 9. Net charges (q) in the different atoms of the title compound.

Atoms	p_v	q_{x-ray}	$q_{ab\ initio}$
O_1	6.25076	–0.25076	–0.69457
C_2	6.23176	–0. 23176	–0.50534
C_3	6.13276	–0. 13276	–0.53473
N_1	5.12076	–0. 12076	–0.52180
C_1	3.93076	0.06924	–0.18991
C_2	4. 01576	–0. 01576	0.36941
C_3	4.01676	–0. 01676	–0.28583
C_4	4.05200	–0.05200	0.20081
C_5	4.05200	–0.05200	–0.27506
C_6	4.05200	–0.05200	–0.19055
C_7	4.13276	–0. 13276	0.11570
C_8	3.97976	0.02024	0.15663
C_9	4.05200	–0.05200	–0.23848
C_{10}	4.05200	–0.05200	–0.20225
C_{11}	3.93076	0.06924	–0.13470
C_{12}	3.93176	0.06824	0.34866
C_{13}	4.05200	–0.05200	–0.28748
C_{14}	4.03376	–0. 03376	0.05188
C_{15}	4.05200	–0.05200	–0.34395
C_{16}	4.10776	–0. 10776	0.72211
C_{17}	4.00476	–0. 00476	–0.72367
H_1	0.80676	0.19324	0.52040
H_3	0.91276	0.08724	0.26146
H_4	0.91276	0.08724	0. 24945
H_5	0.91276	0.08724	0.24893
H_6	0.91276	0.08724	0.24409
H_7	0.85176	0.14824	0.21558
H_9	0.91276	0.08724	0.26002
H_{10}	0.91276	0.08724	0.25161
H_{13}	0.91276	0.08724	0.26638
H_{15}	0.91276	0.08724	0.26658
$H_{17}a$	0.95376	0.04624	0.26077
$H_{17}b$	0.95376	0.04624	0.26049
$H_{17}c$	0.95376	0.04624	0.25897

4.4. Molecular dipole moment

On the basis of the population coefficients of the multipolar density model, the molecule dipole moment could be predicted by using the following equation:

$$\mu = \sum_i q_i r_i + \sum_i \frac{4n+3}{3k_i''}(p_{xi}i + p_{yi}j + p_{zi}k), \quad (3)$$

where r_i is the atomic position, n the number of electrons in the molecule, and Pi are the dipolar electron populations. Dipole moment orientation in the molecule is shown in Fig. 4. There is no paradox between the resulting molecular dipole moment direction and the evaluation of the positive sign of the net charges on the H atoms and the negative sign of the net charges on O, and N atoms. The net charges on the different atoms and the molecular dipole moment are also estimated by *ab initio* (B3LYP/6-31G*) calculations. In this procedure the treatment is restricted to the valence–shell electrons. The results of these calculations are presented in Table 10. From the results, it is shown that the values obtained with x-ray diffraction and the values obtained by theoretical DFT calculations are in agreement. The analysis of the obtained dipole moments shows that the size and direction of the dipole moment vector depend mainly on the position of the substituent, furthermore the orientation of the dipole moment vector is oriented toward 2-hydroxyphenyl.

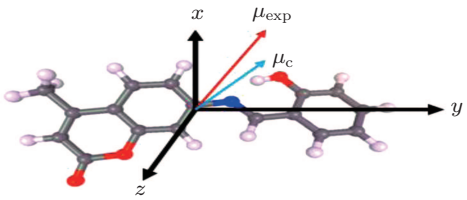


Fig. 4. (color online) Orientation of the molecular dipole moment of the title compound; the origin is at the center of mass of the molecule; μ_{exp}: molecular dipole moment from the multipolar model; μ_c: molecular dipole moment from the *ab initio* calculation.

Table 10. Components of the dipolar moment: x-ray experiment and theoretical *ab initio* calculations.

		μ_x	μ_y	μ_z	μ Debye
Experimental		–0.2171	–0.4577	5.9437	5.9652
Theoretical	(6-31G*B3LYP)	–1.002	–3.1921	1.4912	3.6629
	(HF)	–1.3088	–3.5770	2.6871	4.6613

4.5. Electrostatic potential

As is well known, the electrostatic potential plays a very essential role in the study of the intermolecular interactions of molecular systems. From the obtained continuous charge distribution at a point defined by r', the potential is given by

$$\phi(r') = \int \frac{\rho_{total}(r)}{|r - r'|} dr, \quad (4)$$

in which ρ_{total} represents both the nuclear and the electronic charge. The integration goes over the molecular volume, and r represents the atomic position relative to a common origin.

Figure 5 presents the electrostatic potential distribution around the molecule obtained from the experimental x-ray diffraction data (Fig. 5(a)) and the *ab initio* theoretical calculations. The obtained electrostatic potential as shown in Fig. 5 is composed of the positive electrostatic potential around the 2-hydroxyphenyl groups and the negative electrostatic potential around the coumar in the groups region. This figure also

confirms the nature of the intramolecular charge transfer as determined by the orientation of the molecular dipole moment.

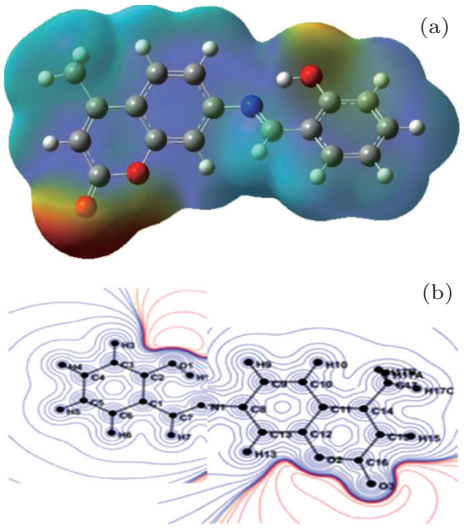


Fig. 5. (color online) Electrostatic potential maps around the molecule. Panel (a) shows the *ab initio* molecular orbital calculations of the electrostatic potential distribution, and panel (b) displays the electrostatic potential distribution predicted from the experimental x-ray diffraction data.

5. Conclusions

In this work, an accurate charge density function is determined in a high resolution crystallographic experiment. This function enables the derivation of some electrostatic molecular proprieties such as the dipole moment and the electrostatic potential on the basis of the multipolar charge density distribution model of Hansen and Coppens as is the case in many previous studies.[16,17]

The structure refinements are achieved by using the multipolar model. All non-hydrogen atoms are refined anisotropically and are subjected to local symmetry constraints. The H atom anisotropic parameters are obtained from thermal motion analysis based on the rigid body bond test. The final reliability factor R is found to decrease until 0.4%. This very low value testifies about the quality of the used experimental data and the efficiency of the multipolar model to describe the electron density distribution in crystals.

Using the MoPro package, a variety of dynamic density deformation maps can be drawn in which the accumulation of the electron charge density along the chemical bonding is shown clearly. It is found that the electron density distribution is almost centered in the middle of the chemical bonds and the oxygen free electron pairs are perfectly localized.

The *ab initio* theoretical structure investigation using the Gaussian 03 package leads to an optimized molecule with bond lengths and bond angles closer to the x-ray experimental results. No significant structural changes are observed compared with the previous results. In general the theoretical electrostatic properties are in good consistence with those derived from the experiment.

Finally, the obtained results indicate the direction of charge transfer within the molecule. The deformation of the electrostatic potential of the title compound shows that the electronegative potential is located on the side of the coumarin group whereas the electropositive potential is on the side of 2-hydroxyphenyl. For a more comprehensive study of the effect of electron charge transfer in this important biological compound, it is recommended to complete the study by performing a vibrational analysis using FT-Raman and FTIR spectroscopic techniques.

References

[1] Silva P S P, Parveen M, Khanam Z, Ali A and Silva M R 2010 *Acta Cryst. E* **66** o988

[2] Nofal Z M, El-Zahar M I and El-Karim S S A 2000 *Molecules* **5** 99

[3] Coppens P 1997 *X-ray Charge Densities and Chemical Bonding* (New York: Oxford)

[4] Spackman M A 1998 *Ann. Rep. Prog. Chem. C.* **94** 177

[5] Aazam E S, Fawazy A and Hitchcock P B 2006 *Acta Cryst. E* **62** o4285

[6] Hansen N K and Coppens P 1978 *Acta Cryst. A* **34** 909

[7] Trueblood K N 1990 *Program THMA11* (Los Angeles: Department of Chemistry and Biochemistry, University of California)

[8] Hirshfeld F L 1976 *Acta Cryst. A* **32** 239

[9] Frisch J, Trucks G W, Schlegel H B, Scuseria G E, Robb M A, Cheeseman J R, Montgomery J A, Vreven J T, Kudin K N, Burant J C, Millam J M, Iyengar S S, Tomasi J, Barone V, Mennucci B, Cossi M, Scalmani G, Rega N, Petersson G A, Nakatsuji H, Hada M, Ehara M, Toyota K, Fukuda R, Hasegawa J, Ishida M, Nakajima T, Honda Y, Kitao O, Nakai H, Klene M, Li X, Knox J E, Hratchian H P, Cross J B, Adamo C, Jaramillo J, Gomperts R,. Stratmann R E, Yazyev O, Austin A J, Cammi R, Pomelli C, Ochterski J W, Ayala P Y, Morokuma K, Voth G A, Salvador P, Dannenberg J J, Zakrzewski V G, Dapprich S, Daniels A D, Strain M C, Farkas O, Malick D K, Rabuck A D, Raghavachari K, Foresman J B, Ortiz J V, Cui Q, Baboul A G, Clifford S, Cioslowski J, Stefanov B B, Liu G, Liashenko A, Piskorz P, Komaromi I, Martin R L, Fox D J, Keith T, Al-Laham M A, Peng C Y, Nanayakkara A, Challacombe M, Gill P M W, Johnson B, Chen W, Wong M W, Gonzalez C and Pople J A 2003 Gaussian 03 (Pittsburgh, Gaussian 03 Revision A.1)

[10] Jelsch C, Guillot B, Lagoutte A and Lecomte C 2005 *J. Appl. Crystallogr.* **38** 1

[11] Hirshfeld F L 1971 *Acta Cryst. B* **27** 769

[12] Hirshfeld F L 1977 *Theor. Chim Acta* **44** 129

[13] Hirshfeld F L and Hope H 1980 *Acta Cryst. B* **36** 406

[14] Baert F, Schweiss P, Heger G and More M 1988 *J. Mol. Struct.* **178** 29

[15] Guillot B 2011 *Acta Cryst. A* **67** C511

[16] Drissi M, Chouaih A, Megrouss Y and Hamzaoui F 2013 *Journal of Crystallography* 2013 ID 326457

[17] Boubegra N, Chouaih A, Drissi M and Hamzaoui F 2014 *Chin. Phys. B* **23** 016103